Materials and Design 157 (2018) 251–257

Contents lists available at ScienceDirect

Materials and Design

journal homepage: www.elsevier.com/locate/matdes

Coherent diffraction study of calcite crystallization during the hydration of tricalcium silicate

Xianping Liu [a,b,c,*], Wei Lin [a], Bo Chen [a,c,d,*], Fucai Zhang [c,d,e], Piqi Zhao [f], Aaron Parsons [g], Christoph Rau [g], Ian Robinson [a,d,h]

[a] School of Materials Science and Engineering, Tongji University, Shanghai 201804, China
[b] Key Laboratory of Advanced Civil Engineering Materials (Tongji University), Ministry of Education, Shanghai 201804, China
[c] Research Complex at Harwell, Rutherford Appleton Laboratory, Didcot, Oxfordshire OX11 0FA, UK
[d] London Centre for Nanotechnology, University College London, London WC1H 0AH, UK
[e] Department of Electrical and Electronic Engineering, Southern University of Science and Technology, Shenzhen 518055, China
[f] Shangdong Provincial Key Laboratory of Preparation and Measurement of Building Materials, University of Jinan, Jinan 250022, China
[g] Diamond Light Source, Rutherford Appleton Laboratory, Didcot, Oxfordshire OX11 0FA, UK
[h] Condensed Matter Physics and Materials Science Department, Brookhaven National Laboratory, Upton, NY 11973, USA

HIGHLIGHTS

- Calcite crystallization during the carbonation at the nano-scale in 3D was successfully studied by BCDI.
- Calcite crystallization follows a through-solution reaction, which is supported by our findings.
- Calcite crystals grow by increasing the number of phase domains while the domain size remains at about 200~300nm.

GRAPHICAL ABSTRACT

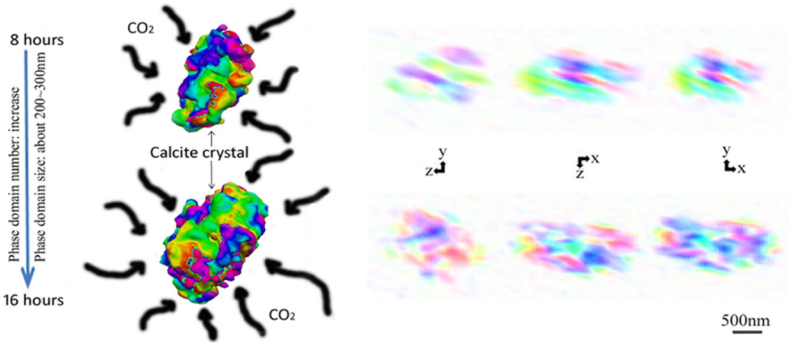

ARTICLE INFO

Article history:
Received 14 April 2018
Received in revised form 13 July 2018
Accepted 14 July 2018
Available online 17 July 2018

Keywords:
Carbonation
Bragg coherent X-ray diffraction imaging (BCDI)
Calcite crystallization
Tricalcium silicate (C_3S)

ABSTRACT

The aim of this work is using Bragg coherent X-ray diffraction imaging (BCDI) to study the calcite crystallization during carbonation of hydrated tricalcium silicate (C_3S). Portland cement is a very complex synthesized product whose 50–70% mass is composed of C_3S, which is the most important phase to produce calcium silicate hydrates and calcium hydroxide. Hence, its hydration contributes greatly to the hydration of cement and later to the carbonation of cement products when it reacts with CO_2, often from the air, to form calcium carbonates. BCDI has emerged in the last decade as a promising high-resolution lens-less imaging approach for characterization of various samples. It has made significant progress with the development of X-ray sources and phase-retrieval algorithms. BCDI allows for imaging the whole three-dimensional structure of micro- and sub-micro- crystalline materials and can show the strain distribution at the nanometer spatial resolution. Results show that calcite crystallization follows a through-solution reaction and the growth model of the calcite crystal can be explained by using "phase domain" theory. During carbonation, calcite crystals grow by increasing the number of phase domains within them while the domain size remains at about 200–300 nm.

* Corresponding authors at: School of Materials Science and Engineering, Tongji University, Shanghai 201804, China.
E-mail addresses: lxp@tongji.edu.cn (X. Liu), bo.chen@tongji.edu.cn (B. Chen).

https://doi.org/10.1016/j.matdes.2018.07.031
0264-1275/

1. Introduction

The mechanism of cement hydration has been largely investigated and discussed [1–4]. Portland cement, the most commonly used cement mixture, contains four major phases: tricalcium silicate (Ca_3SiO_5 or simplified as C_3S), dicalcium silicate (Ca_2SiO_4 or simplified as C_2S), tricalcium aluminate ($Ca_3Al_2O_6$, or simplified as C_3A), and tetracalcium aluminoferrite (Ca_2AlFeO_5, or simplified as C_4AF). In production clinkers, due to incorporation of substituent ions, they exist as alite, belite, aluminate and ferrite. The substituent ions for Ca^{2+}, such as Mg^{2+}, Al^{3+} and Fe^{3+}, will improve the reactivity of those clinker phases. The clinker is mixed with a few per cent of calcium sulfate and finely ground, to make the Portland cement. Some specifications allow the addition of other materials at the grinding stage, such as limestone. There about 50–70% of cement mass is C_3S, 15–30% is C_2S, 5–10% is C_3A and 5–15% is C_4AF, in which C_3S is the most important hydraulic phase [5]. C_3S reacts relatively quick with water, usually reaching about 70% completion within 28 days. The hydration of C_3S contributes the most to the strength development of the hardened cement paste.

The hydration of C_3S is shown as following:

$$C_3S + nH_2O \rightarrow xCaO \cdot SiO_2 \cdot yH_2O + (3-x)\,Ca(OH)_2 \quad (1-1)$$

where x is the mole ratio of calcium oxide to silica (simplified as C/S), y is the mole ratio of water to silica (simplified as H/S). $xCaO \cdot SiO_2 \cdot yH_2O$ is usually abbreviated as C-S-H. $Ca(OH)_2$ is usually abbreviated as CH.

There are two types of C-S-H. The first type is C-S-H(I) with the C/S between 0.8 and 1.5 and H/S between 0.5 and 2.5. The second type is C-S-H(II) with the C/S between 1.5 and 2.0 and H/S between 1 and 4. The increased water to cement ratio (simplified as w/c), the longer hydration time and the adding of mineral additions will decrease the C/S of C-S-H.

Calcium hydroxide ($Ca(OH)_2$, or simplified as CH), called portlandite in its mineral form, is one of the main products generated from the hydration of C_3S. It crystallizes when the pore solution of the hydrated cement is supersaturated. The growth of CH is an important indication of the beginning of the main hydration period of C_3S.

The chemical reactions taking place in Portland cement are generally more complex than simple conversions of anhydrous compounds into the corresponding hydrates. The hydrates of Portland cement include not only corresponding hydrates of the four major phases, but also those from the reactions with calcium sulfate and other additions, such as AFt, AFm, etc.

CH will react with CO_2, often from the atmosphere, to form calcium carbonates ($CaCO_3$). This is the conventional definition of carbonation in cement chemistry. In fact, it has been noticed that the main cement hydration product, C-S-H and unhydrated cement components C_3S, C_2S can also consume a certain amount of CO_2, and get involved in the carbonation process [6]. When C-S-H reacts with CO_2 or CO_3^{2-} ions with formation of $CaCO_3$, The C/S of the C-S-H will decrease and finally C-S-H is destroyed into hydrous silica. Vaterite and aragonite are formed when C-S-H of low C/S is exposed to CO_2 [7].

The carbonation of CH and C-S-H are shown as followings:

$$CH + CO_2 + nH_2O \rightarrow CaCO_3 + (n+1)H_2O \quad (1-2)$$

$$C-S-H + CO_2 + H_2O \rightarrow CaCO_3 + SiO_2 \cdot 2H_2O \quad (1-3)$$

The replacement of low molar volume CH by the high molar volume higher-strength $CaCO_3$ could decrease the porosity and consolidate the microstructure of the hardened cement paste, and thus increase its strength [8]. Unfortunately, if there were too much CO_2 taken up by the hardened cement paste, the CH could be depleted. Overconsumption of the CH will cause the decrease of the alkalinity in the cement pore solution and hence damage the passive film on the reinforcement steel bars (used in concrete), which leads to the corrosion of these rebars [9]. Keeping a certain amount of CH in the hydrated cement is essential to prevent the corrosion of the rebars by maintaining the alkalinity in the pore solution. The decalcification-polymerization process of C-S-H will also do harm to the microstructure and hence decrease the performance of hardened cement paste. Furthermore, if there were too much $CaCO_3$ formed in the hydrated cement, it could lead to the carbonation shrinkage of hardened cement paste and even cause cracking due to the water released [10].

The carbonation mechanism is well understood from a physicochemical point of view [11–14]. And the polymorphism of formed $CaCO_3$ (calcite, vaterite, aragonite) has been studied a lot [15–18].

Slegers et al. studied the carbonation of the hydrates of C_3S by infrared (IR) spectroscopy combined with X-ray powder diffraction (XRPD) analysis [19]. The results show that the carbonation finally leads to the complete disappearance of the C-S-H gel and the retention of identifiable amount of CH. Hence, it is concluded that C-S-H gel is easier to be carbonated than CH [19]. There are three crystal forms of $CaCO_3$: calcite, aragonite, and vaterite, in which calcite is the most abundant one in nature. In the results from Slegers et al., $CaCO_3$ were found to be vaterite and aragonite, with only small amounts in the form of calcite [19]. This research also showed that in case that the (hydrated) C_3S samples had a lower degree of hydration, the aragonite would be the main carbonation product. While for the samples with higher degree of hydration, vaterite would be the main carbonation product, and the formed silica is in an amorphous state [19].

On the other hand, Villain et al. found that $CaCO_3$ generated from CH is mainly calcite, and the $CaCO_3$ generated from C-S-H is less stable because it usually composed by a great amount of poorly crystallized vaterite and aragonite [20]. This is consistent with the results from Šauman et al. [21] and Grandet et al. [22]. Furthermore, in the work by Villain et al., it found by thermogravimetric analysis-chemistry analysis (TGA-CA) and Fourier transform infrared (FT-IR) spectroscopy analysis that CH remains in the "fully" carbonated material as an uncarbonated CH crystal nucleus covered by a dense carbonated layer of $CaCO_3$, and C-S-H begins to carbonate before the "full" consumption of CH [20, 22]. This is different from the results obtained by Slegers et al. [19]. Other research shows that the CH and C-S-H carbonate simultaneously [23].

Besides the above anhydrous crystalline phases of $CaCO_3$, there are two hydrated crystalline phases, i.e. ikaite ($CaCO_3 \cdot 6H_2O$) and monohydrocalcite ($CaCO_3 \cdot H_2O$). They are metastable intermediate phases affecting the crystal size, shape, and structure of calcite [24, 25].

These studies indicate that different experimental conditions could lead to different conclusions. However, the exact visual crystallization mode of $CaCO_3$ during cement hydration is unclear, leading to the difficulty of quantifying its effect to the microstructure and hence performance variation of the cement materials during application. Furthermore, the control of the growth of $CaCO_3$ crystals is still a subject of research, and even debate. Therefore, the carbonation of cement attracts lots of attention from researchers.

In this work, we used Bragg coherent X-ray diffraction imaging (BCDI) to probe the crystallization process of one of the polymorphism of formed $CaCO_3$, calcite, during the carbonation in the hydrated C_3S in order to further enrich the knowledge about the carbonation mechanism at the nano-scale in three dimensions. BCDI is an advanced form of dark-field X-ray microscopy: a coherent X-ray beam is focused onto the sample from a high-brightness source of synchrotron radiation. Under these conditions, the Bragg diffraction peaks of every crystallite in the sample contain intensity fringes whose spacing is inversely proportional to the distance between the crystal edges in that direction. The missing phase of the coherent diffraction patterns is then reconstructed by using iterative phase retrieval algorithms to form an image [26–29]. The resulting three-dimensional (3D) images of the crystals and the inner strain distribution within them takes advantage of the sensitivity of the X-rays to the distortions of crystalline lattice, to obtain not only the 3D images of individual crystals at nano-scale, but also

crystal defects and strain fields inside crystals seen as phase [30–34]. It has been applied to study behaviors of various (nano-)crystalline samples including calcite crystals as well [35, 36]. The reconstructed results from BCDI are function of a complex variable [26], with the amplitude representing the electron density contribution to a particular Bragg peak and phase (shift) representing the strain/internal deformation in the crystal lattice [26]. From our BCDI experiment on observing the formation of calcite crystals in the hydrated C_3S powder, during carbonation, we found that the calcite crystal grows in a multiple domain mode, which enriches the carbonation mechanism of hydrated cement materials.

2. Experimental methods

Pure C_3S powder was prepared at the School of Materials Science and Engineering, Tongji University by following the same experimental procedure reported by De la Torre & Aranda [37]. All the raw materials (from Sinopharm Chemical Reagent Co., Ltd) $CaCO_3$, $Mg(OH)_{2.4}MgCO_{3.5}H_2O$, SiO_2 and Al_2O_3 were measured according to the stoichiometric ratio $Ca_{2.92}Mg_{0.06}O_3(SiO_2)_{0.98}(Al_2O_3)_{0.02}$. The XRD powder pattern was analyzed by Rietveld methodology using Topas software to obtain Rietveld Quantitative Phase Analysis (RQPA). The sample contains 83.13 wt% of monoclinic C_3S, 13.91 wt% of rhombohedric C_3S, 1.73 wt% of β-C_2S and 1.23 wt% of f-CaO. Fig. 1 gives Rietveld plots for the raw material.

The dry C_3S powder was mixed with pure water at ratio 0.5 by weight. The mixed paste was drop-cast onto a piece of silicon wafer, and sealed in a plastic bag to avoid water evaporation. It was left for hydration for 7 days in the sealed bag in a glove box. Then the sample was taken out from the bag and kept in air for 14 days at room temperature for natural carbonation. The concentration of carbon dioxide in the air is about 0.038% by volume, in which condition the carbonation happened very slow. 8 h before the first BCDI measurement, the wet sample was transferred to the bottom of a container filled with freshly made solution of ammonium carbonate. Since the density of CO_2 is 1.52 times of that of the air, CO_2 enriched at the bottom of the container and completely soaked the sample. This creates an atmosphere with rich CO_2 that can be absorbed by the sample, which could accelerate the carbonation in a reasonable limit of time. The accelerated carbonation at high CO_2 leads to a preferential formation of $CaCO_3$ crystals on the surface of CH particles [38]. The sample was then removed from the artificial CO_2 atmosphere and installed on the sample holder to be measured by the BCDI to see the growth of calcite crystals. A second measurement made on the same crystal after another 8 hour exposure of the sample to the ammonium carbonate solution environment.

The coherence branch of the beamline I-13 of the Diamond Light Source was used to perform the experiment [39]. Fig. 2 shows the schematic BCDI experiment setup at the beamline I-13 of the Diamond Light Source. The X-ray energy was set to 9.7 keV by a horizontal-bounce double crystal monochromator using Si (111) crystals. The coherent beam was selected by a pinhole which was centered over the axis of an air-bearing rotation stage. The stage was also used as the theta axis for scanning the Bragg peaks. An XYZ stack of piezo stage was used to position the sample with sub-micron accuracy in the beam.

A three-ball kinematic-mount magnetic chuck, with about 1 micron accuracy of position repetition, was used to hold the samples. This allowed the interchange of the samples and the excellent relocation afterwards, and it is very important because of the need to repeat the measurement of the same crystal in the sample after its further treatment for comparison. A confocal microscope was installed over the sample holder as well. For the first measurement, after the targeted crystal was well centered in the X-ray beam and ready for measurement, the confocal microscope was aligned to focus on the crystal, and then the position of the crystal in the confocal microscope was recorded and the confocal microscope was kept static. When we were doing the following measurements, and mounted the same sample back to the holder, the height of the sample was varied until the targeted crystal was re-focused in the confocal microscope, and the crystal was then brought back to the same position previously recorded in the confocal microscope by moving the sample stage, so that the position of the (measured) crystals could be accurately reproduced [40]. The set-up also facilitated centering of the theta axis in the beam. The sample was aligned "flat" in the beam by using the total reflection from the silicon wafer. It was then tilted forward by 2° to let the X-rays illuminate the center of the wafer.

A Merlin detector, consisting of four X-ray counting MedPix-3 chips in a 2×2 array, was used to record the diffraction patterns. The detector was mounted on an adjustable frame at an in-plane angle (delta) of 26.5° and an out-of-plane angle (gamma) of 15.1° with a sample-to-detector distance of 2.05 m. The MediPix-3 chips have pixels of 55 × 55 microns. The exact detector 2θ angle was calibrated with a standard powder sample of calcite, first locating the (stronger) {0-14} ring at 24.31°, then moving to the {006} Bragg reflection at 25.99°.

Bragg peaks from the hydrated C_3S sample were found at the same angle on the detector as the standard calcite. Each diffraction pattern corresponding to a different crystal that happened to be at the correct angle for Bragg diffraction was aligned to maximize the signals recorded by the detector. Then a full rocking curve of 2D diffraction patterns was recorded by theta scans, usually with step of 0.003° to sufficiently oversample the diffraction pattern. The 3D stack records the full volume of reciprocal space surrounding the Bragg peak. The data were extracted from the original .hdf file, then cropped to the region covered the target peak only to remove the other unrelated diffraction. This 3D array of intensity was directly used as the input of the BCDI phasing algorithm [35].

Inversion of the BCDI data into 3D images in our work was done by methods [26] based on the Fienup's Hybrid Input-Output (HIO) method [28] plus a "shrinkwrap" algorithm until it was close to the real crystal

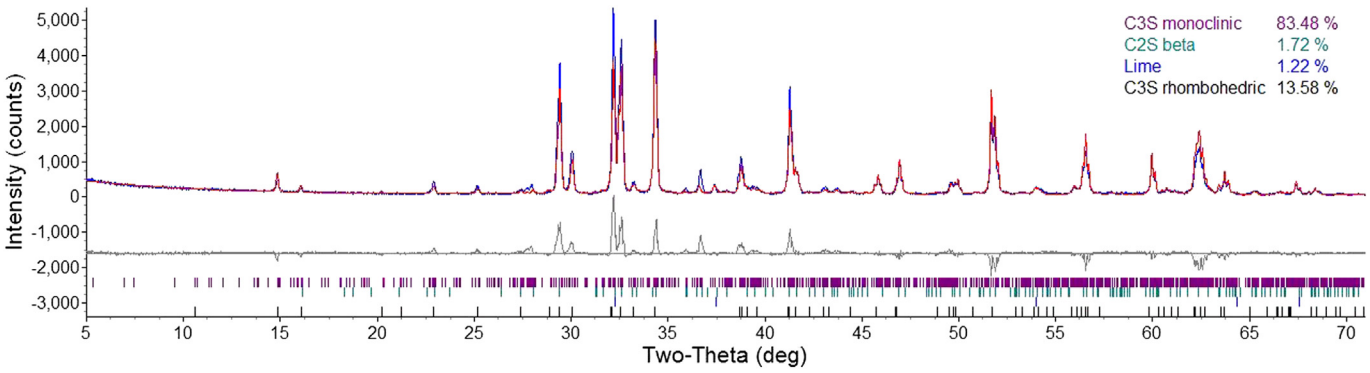

Fig. 1. Rietveld plots for anhydrous C_3S sample with the observed (blue line), calculated (red line) and difference (bottom line) powder patterns. (For interpretation of the references to color in this figure legend, the reader is referred to the web version of this article.)

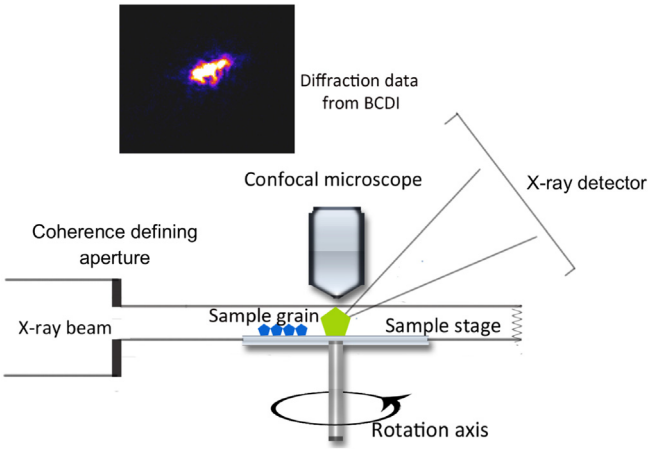

Fig. 2. Schematic BCDI experiment setup at the beamline I-13 of the Diamond Light Source.

size [41]. The sample strain is interpreted as the phase at each location in the reconstructed 3D images. This phase $\Delta\varphi$ corresponds to a projection of the local crystal displacement vector **u**, according to the relation [26], $\Delta\varphi = \mathbf{Q} \cdot \mathbf{u}$, where **Q** is the momentum transfer vector of the measured Bragg peak.

The reconstructed images were viewed as "isosurface" contour, which was colored according to the phase values. The amplitude of the 3D real-space images is interpreted as "Bragg density", which is the local strength of that region of the crystal for contributing the diffraction to the Bragg peak, and it is not the same as its physical density [42]. This is somewhat analogous to the dark-field contrast mechanism in TEM.

3. Results and discussion

3.1. Diffraction patterns of the crystal

We deliberately exposed the sample to CO_2 to observe the formation of calcite crystals in the hydrated C_3S powder. Fig. 3 represents the diffraction patterns of a {0-14} calcite peak at the Bragg angle 24.31° from the sample exposed to the artificial CO_2 environment for 8 h (a) and for 16 h (b). Clearly, the center of the Bragg diffraction peak in Fig. 3(b) is more concentrated and smaller than that in Fig. 3(a), which means the crystal has grown bigger.

3.2. Characterization of the crystal structure

Fig. 4 shows a reconstructed image of the calcite by the BCDI measurement, in which Fig. 4(a) shows the shape of the calcite crystal after being exposed to CO_2 for 8 h, and Fig. 4(b) for 16 hour exposure. Fig. 5 shows cross sections on the XY planes of the two reconstructed 3D images as shown in Fig. 4. In Fig. 5, the density is coded in color, the higher the value in the color bar, the higher the density of the crystalline material in the sample. From panels (a) to (b) in both Figs. 4 and 5, the growth of the calcite crystal during carbonation is clearly demonstrated. The calcite crystal, experienced 8 h exposure to the artificial CO_2 atmosphere, has grown from 2388 nm × 1422 nm × 890 nm to 2922 nm × 1671 nm × 1263 nm (in length, width and height) after a further 8 h of CO_2 treatment. The directions used for measuring the length, width and height of the crystal were shown in the black coordinate axes with L, W and H on the right of Fig. 4, in which L stands for the length direction, W for the width direction and H for the height direction.

Generally, there are two mechanisms for the formation of crystals during the reaction process of cement: topochemical reaction [43] and through-solution reaction [44]. Carbonation is believed to be a through-solution reaction because $CaCO_3$ is produced by CO_3^{2-} ions from the dissolved CO_2 in the pore solution and Ca^{2+} ions from the dissolved hydrates, such as CH [45] and from the C-S-H with lowered Ca/Si ratio [46]. From the above measurement, we can see that after 8 h CO_2 treatment, the calcite crystal grew 22% and 18%, respectively, along the length and width directions with a similar rate. Differently, along the height direction, on the length-width plane, it grew 42%, which was almost as twice faster as along the other 2 directions. This is an evidence that calcite crystallization/formation is a through-solution reaction whose rate largely influenced by the surface area because, in the target calcite crystal, the length-width plane with dimensions of 2388 nm × 1422 nm was much larger than the other 2 planes with dimensions of 2388 nm × 890 nm and 1422 nm × 890 nm, and the calcite crystal grew much faster on larger plane (see Fig. 4 as well).

3.3. Domain formation within the crystal

It is clear from the images above that there is substantial disorder in the form of density (Fig. 5) and strain (Fig. 4) distribution in the grown calcite crystal. The outer surface of the crystal can be seen in Fig. 4, which is composed of small blocks with roughly constant phase. We identify these as phase domains, i.e. regions of material that are uniform in chemical composition and physical state. However, they are having different phase in the image, so must be physically shifted differently with respect to the imaging Q-vector, because the phase is the

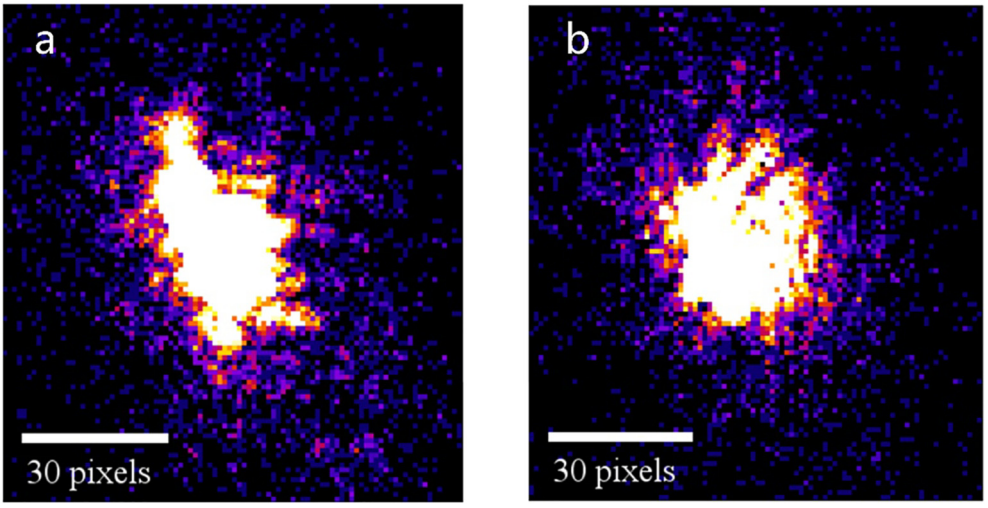

Fig. 3. Coherent X-ray diffraction patterns from a crystalline calcite {0-14} peak at the Bragg angle 24.31°, after the sample exposure to CO_2 for 8 h (a) and 16 h (b).

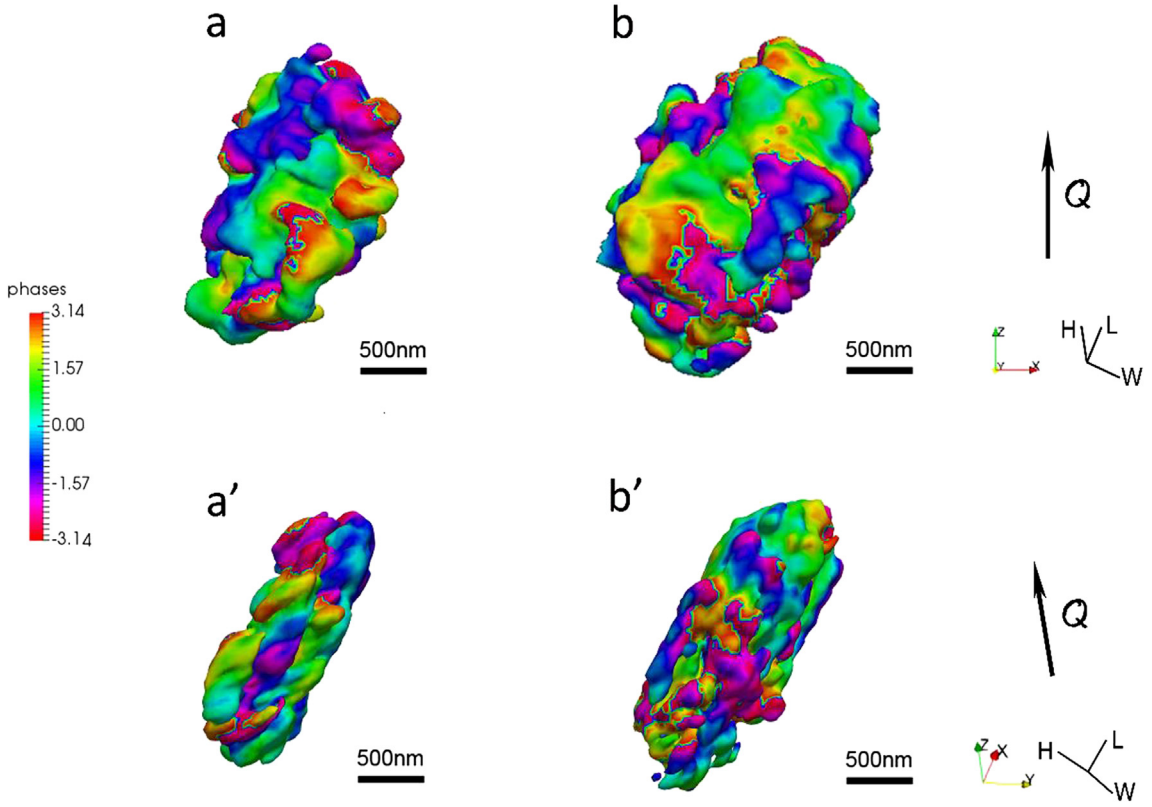

Fig. 4. Isosurface view of the reconstructed images of a crystalline calcite growing within the hydrated C_3S powder sample after exposure to CO_2 for 8 h (a) & (a′) and 16 h (b) & (b′). Panels a and a′ are the two views of the same image from different orientations, panels b and b′ are also the two views of the same image from different orientations. The isosurface has been color-coded according to the phase value at each position in the images. The black coordinate axes with L, W and H stand for the directions used for the measurement of the length, width and height of the crystal. (For interpretation of the references to color in this figure legend, the reader is referred to the web version of this article.)

projection of the lattice displacement onto Q, given by $\Delta\varphi = \mathbf{Q} \cdot \mathbf{u}$, as mentioned above [26]. This can be better presented as cross sections using the HSV color scheme as shown in Fig. 6, in which different colors represent different phase domains. HSV is named as such for three values: hue, saturation, and value, which describes colors (hue or tint) in terms of their shade (saturation or amount of gray) and their brightness value. Here, density is represented by saturation and phase is represented by color, so only the strongly diffracting regions appeared in the images. Fig. 6 shows the internal phase domains of the calcite crystal after being exposed to CO_2 for 8 h (a, b, c) and for 16 h (d, e, f). The small blocks with almost constant phase are seen to penetrate throughout the volume of the crystal. It is clear from the result that the number of domains is increasing in time while the domain size is staying roughly constant at 200–300 nm.

4. Conclusions

Bragg coherent X-ray diffraction imaging (BCDI) was used to observe the growth and crystallization mode of one of the polymorphism of formed $CaCO_3$, a calcite crystal, within the hydrated C_3S paste. C_3S

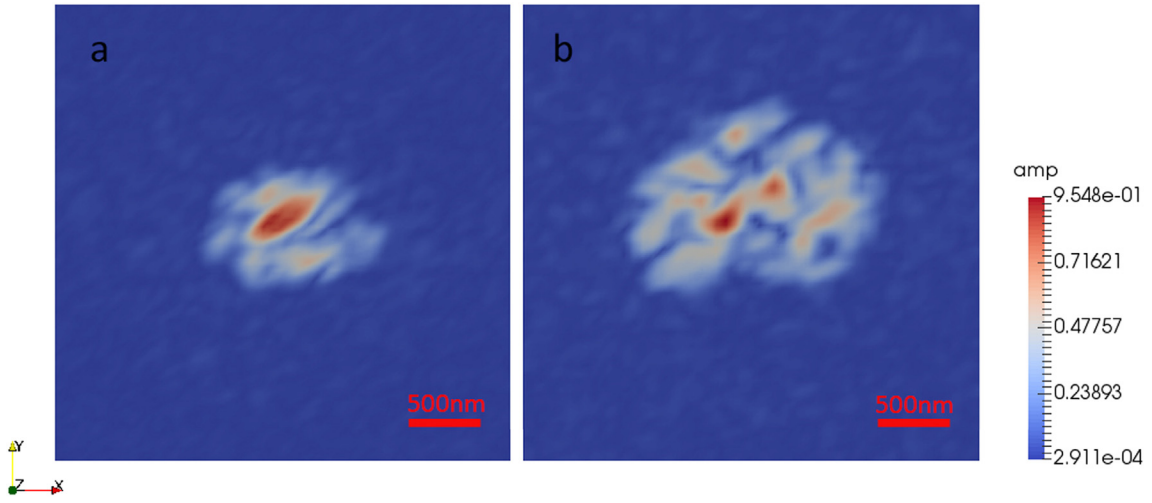

Fig. 5. Cross sections of the reconstructed 3D images of the crystalline calcite, the same crystal as shown in Fig. 3, which was exposed to CO_2 for 8 h (a) and 16 h (b). The amplitude of the image is represented by a color scale. (For interpretation of the references to color in this figure legend, the reader is referred to the web version of this article.)

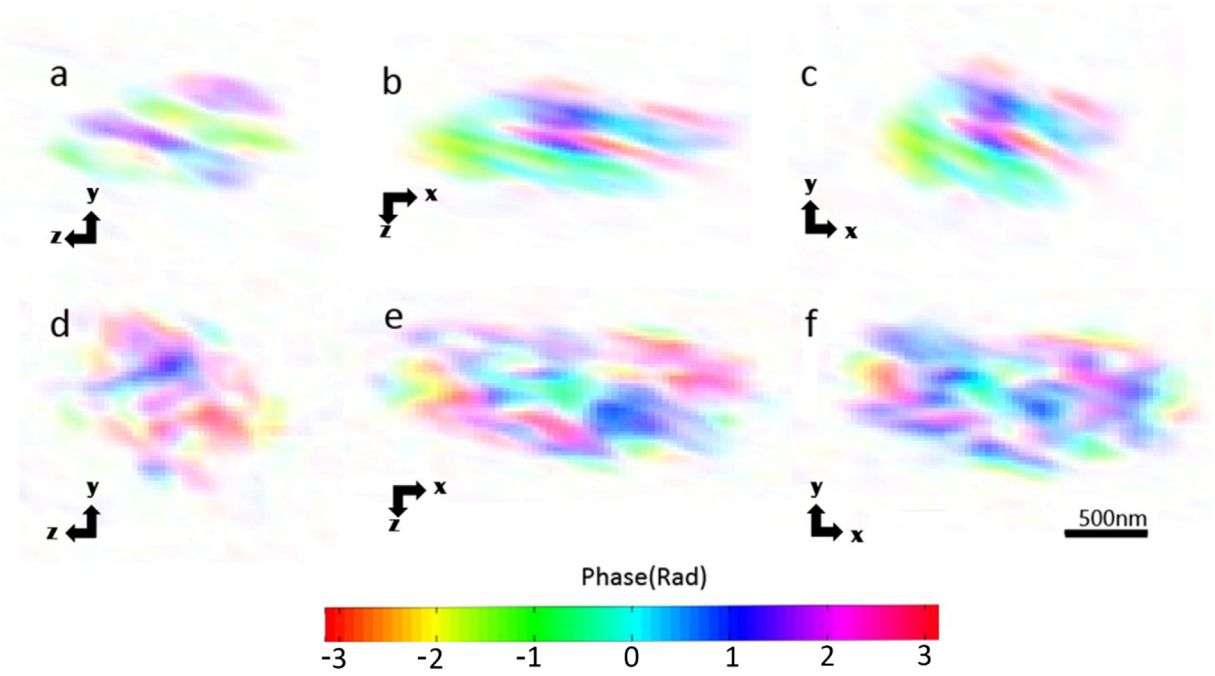

Fig. 6. Cross sections of the grown calcite crystal after the hydrated C_3S sample was exposed to CO_2 for 8 h (a, b, c) and 16 h (d, e, f). The images were color-coded by the phase value using the HSV color scheme to illustrate the phase domains. (For interpretation of the references to color in this figure legend, the reader is referred to the web version of this article.)

powder was mixed with water, hydrated for 7 days and kept in the air for 14 days for natural carbonation. The sample was then exposed to the artificial CO_2 environment for 8 h before the first measurement, and 16 h before the second measurement. From the BCDI investigation of the crystallization behavior of the calcite during the C_3S hydration process, the following conclusion can be drawn:

(1) BCDI is a mature method to investigate behaviors of a fixed form of crystal. This is the first time BCDI has been used to observe the calcite crystallization during the hydration of a C_3S paste which is a typical simplified model of the cement paste. We clearly observed the calcite crystal grows bigger with time goes from the first measurement to the second one in three-dimensions.
(2) Our work provides an evidence supports that calcite crystallization/formation is a through-solution, and the crystal growth rate is controlled by the surface areas of the growing crystal itself.
(3) The calcite crystal grown in this way is not perfect, but made up of distinct phase domains. The calcite, formed by the reaction of CO_2 with the hydrate, grows by increasing the number of phase domains while the domain size almost remains the same at around 200–300 nm.

The above results will help us to optimize the curing conditions and hence control the effect of carbonation on the properties of materials from the aspect of crystallization direction and strain distribution of the calcite.

Author contributions

Xianping Liu, Ian Robinson and Bo Chen conceived the project. Piqi Zhao synthesized and analyzed the C_3S samples with XRD. Xianping Liu, Ian Robinson, Bo Chen, Fucai Zhang, Aaron Parsons and Christoph Rau carried out the BCDI experiment. Wei Lin and B.C. analyzed the data. Xianping Liu, Wei Lin, Ian Robinson and Bo Chen wrote the manuscript with contributions from all the other co-authors.

Acknowledgment

This work was supported by the Tongji University's Talent Program "Materials Nanostructure" with grants 152221 and 152243, and the UK Engineering and Physical Sciences Research Council (EPSRC) grant EP/I022562/1 "Phase modulation technology for X-ray imaging". Work performed at Brookhaven National Laboratory was supported by the U.S. Department of Energy, Office of Basic Energy Sciences, under Contract Number DE-SC00112704. Part of the work at Tongji University was also supported by National Natural Science Foundation of China (Project 51102181). Xianping Liu was supported by the State Scholarship Fund of China when implementing the experiment. The BCDI experiment was carried out at the coherence branch of the beamline I-13 of the Diamond Light Source.

Conflict of interest

The authors declare no potential conflicts of interest with respect to the research, authorship, and/or publication of this article.

Data availability

The datasets generated during the current study are available from the corresponding author on reasonable request.

Appendix A. Supplementary data

Supplementary data to this article can be found online at https://doi.org/10.1016/j.matdes.2018.07.031.

References

[1] H.F.W. Taylor, P. Barret, P.W. Brown, D.D. Double, G. Frohnsdorff, V. Johansen, D. Ménétrier-Sorrentino, I. Odler, L.J. Parrott, J.M. Pommersheim, M. Regourd, J.F. Young, Mater. Struct. 17 (1984) 457–468.
[2] E.M. Gartner, J.M. Gaidis, Hydration mechanisms, I, in: J. Skalny (Ed.), Materials Science of Concrete, vol. 1, American Ceramic Society, Westerville, OH 1989, pp. 95–125.

[3] J.M. Gaidis, E.M. Gartner, Hydration mechanisms, II, in: J. Skalny, S. Mindess (Eds.), Materials Science of Concrete, vol. 2, American Ceramic Society, Westerville, OH 1989, pp. 9–39.
[4] E.M. Gartner, J.F. Young, D.A. Damidot, I. Jawed, Hydration of Portland Cement, in: J. Bensted, P. Barnes (Eds.), Structure and Performance of Cements, 2nd ed.Spon Press, New York 2002, pp. 57–113.
[5] H.F.W. Taylor, Cement Chemistry, 2nd ed. Thomas Telford Publishing, London, 1997 1–2.
[6] V.G. Papadakis, C.G. Vayenas, M.N. Fardis, ACI Mater. J. 88 (1991) 363–373.
[7] A. Morandeau, M. Thiéry, P. Dangla, Cem. Concr. Res. 56 (2014) 153–170.
[8] F.W. Locher, Cement-Principles of Production and Use, Verlag Bau + Technik GmbH, Düsseldorf, 2006 325.
[9] S. Keysar, D. Hasson, R. Semiat, D. Bramson, Ind. Eng. Chem. Res. 36 (1997) 2903–2909.
[10] B. Šavija, M. Luković, Constr. Build. Mater. 117 (2016) 285–301.
[11] Q.T. Phung, N. Maes, D. Jacques, G. De Schutter, G. Ye, J. Perko, Constr. Build. Mater. 114 (2016) 333–351.
[12] A.B. Ribeiro, T. Santos, A. Goncalves, Constr. Build. Mater. 175 (2018) 360–370.
[13] S. Kashef-Haghighi, Y.X. Shao, S. Ghoshal, Cem. Concr. Res. 67 (2015) 1–10.
[14] Z.G. Shi, B. Lothenbach, M.R. Geiker, J. Kaufmann, A. Leemann, S. Ferreiro, J. Skibsted, Cem. Concr. Res. 88 (2016) 60–72.
[15] H. Choi, H. Choi, M. Inoue, R. Sengoku, Appl. Sci. Basel 7 (2017) 546.
[16] Y.P. Zeng, J.W. Cao, Z. Wang, J.W. Guo, J.S. Lu, Cryst. Growth Des. 18 (2018) 1710–1721.
[17] C.C. Wu, Z.M. Sun, L.S. Liu, Analyst 142 (2017) 2547–2551.
[18] R. Chang, S. Kim, S. Lee, S. Choi, M. Kim, Y. Park, Front. Energy Res. 5 (2017) 1–12.
[19] P.A. Slegers, P.G. Rouxhet, Cem. Concr. Res. 6 (1976) 381–388.
[20] G. Villain, M. Thiery, G. Platret, Cem. Concr. Res. 37 (2007) 1182–1192.
[21] Z. Šauman, Cem. Concr. Res. 1 (1971) 645–662.
[22] J. Grandet, Contribution à l'étude de la Prise et de la Carbonation des Mortiers au Contact des Matériaux Poreux, Ph.D. Dissertation Université Paul Sabatier, Toulouse, 1975.
[23] A.M. Dunster, Adv. Cem. Res. 2 (1989) 99–106.
[24] R. Besselink, J.D. Rodriguez-Blanco, T.M. Stawski, L.G. Benning, D.J. Tobler, Cryst. Growth Des. 17 (2017) 6224–6230.
[25] S. Sanchez-Moral, J.C. Canaveras, L. Laiz, C. Saiz-Jimenez, J. Bedoya, L. Luque, Geomicrobiol J. 20 (2003) 491–500.
[26] I. Robinson, R. Harder, Nat. Mater. 8 (2009) 291–298.
[27] J.N. Clark, L. Beitra, G. Xiong, A. Higginbotham, D.M. Fritz, H.T. Lemke, D. Zhu, M. Chollet, G.J. Williams, M. Messerschmidt, B. Abbey, R.J. Harder, A.M. Korsunsky, J.S. Wark, I.K. Robinson, Science 341 (2013) 56–59.
[28] J.R. Fienup, Appl. Opt. 21 (1982) 2758–2769.
[29] J. Miao, P. Charalambous, J. Kirz, D. Sayre, Nature 400 (1999) 342–344.
[30] B. Abbey, JOM 65 (2013) 1183–1201.
[31] M.A. Pfeifer, G.J. Williams, I.A. Vartanyants, R. Harder, I.K. Robinson, Nature 442 (2006) 63–66.
[32] M.A.G. Aranda, F. Berenguer, R.J. Bean, X. Shi, G. Xiong, S.P. Collins, C. Nave, I.K. Robinson, J. Synchrotron Radiat. 17 (2010) 751–760.
[33] R. Harder, I.K. Robinson, JOM 65 (2013) 1202–1207.
[34] S.J. Leake, V. Favre-Nicolin, E. Zatterin, M.-I. Richard, S. Fernandez, G. Chahine, T. Zhou, P. Boesecke, H. Djazouli, T.U. Schülli, Mater. Des. 119 (2017) 470–471.
[35] J.N. Clark, J. Ihli, A.S. Schenk, Y.Y. Kim, A.N. Kulak, J.M. Campbell, G. Nisbet, F.C. Meldrum, I.K. Robinson, Nat. Mater. 14 (2015) 780–784.
[36] J. Ihli, J.N. Clark, A.S. Côté, Y.Y. Kim, A.S. Schenk, A.N. Kulak, T.P. Comyn, O. Chammas, R.J. Harder, D.M. Duffy, I.K. Robinson, F.C. Meldrum, Nat. Commun. 7 (2016) 11878.
[37] A.G. De la Torre, M.A.G. Aranda, J. Appl. Crystallogr. 36 (2003) 1169–1176.
[38] J.R. Johnstone, F.P. Glasser, 9th ICCCC; New Dehli, 5, 1992 370–376.
[39] C. Rau, U. Wagner, A. Peach, I.K. Robinson, B. Singh, G. Wilkin, C. Jones, SRI 2009: the 10th international conference on synchrotron radiation instrumentation, in: R. Garrett, I. Gentle, K. Nugent, S. Wilkins (Eds.), AIP Conference Proceedings 1234, American Institute of Physics, New York 2010, pp. 121–125.
[40] L. Beitra, M. Watari, T. Matsuura, N. Shimamoto, R. Harder, I. Robinson, SRI 2009: the 10th international conference on synchrotron radiation instrumentation, in: R. Garrett, I. Gentle, K. Nugent, S. Wilkins (Eds.), AIP Conference Proceedings 1234, American Institute of Physics, New York 2010, pp. 57–60.
[41] S. Marchesini, H. He, H.N. Chapman, S.P. Hau-Riege, A. Noy, M.R. Howells, U. Weierstall, J.C.H. Spence, Phys. Rev. B 68 (2003), 140101. .
[42] X. Liu, M.A.G. Aranda, B. Chen, P. Wang, R. Harder, I. Robinson, Cryst. Growth Des. 15 (2015) 3087–3091.
[43] V. Kohlschütter, P. Haenni, Z. Anorg. Allg. Chem. 105 (1918) 121–144.
[44] H. Le Chatêlier, Recherches Expérimentales sur la Constitution des Mortiers Hydrauliques, Ph.D. Dissertation École des Mines, Paris, 1887.
[45] M. Thiery, G. Villain, P. Dangla, G. Platret, Cem. Concr. Res. 37 (2007) 1047–1058.
[46] H.F.W. Taylor, Cement Chemistry, 2nd ed. Thomas Telford Publishing, London, 1997 357.